Optical distance measurements at two wavelengths with air refractive index compensation

Joffray Guillory, Daniel Truong, Jean-Pierre Wallerand

Conservatoire national des arts et métiers (Cnam), Laboratoire Commun de Métrologie LNE-Cnam (LCM), LNE, 1 rue Gaston Boissier, 75015 Paris, France, (joffray.guillory@cnam.fr; daniel.truong@cnam.fr; jean-pierre.wallerand@cnam.fr)

ABSTRACT

We present our first results in the realization of an absolute distance meter that will bring well-defined and metrologically traceable measurements for distances of several kilometers. The purpose is to achieve an accuracy of 1 mm up to 5 km and beyond. To this end, the developed prototype operates at two different wavelengths, 780 nm and 1560 nm. For each of these wavelengths, the measured distance is determined from the phase accumulated by a radio-frequency carrier propagated in air by a laser beam modulated in intensity. Thus, using the dispersion relation between these two measurements, a compensation of the refractive index of air can be applied, *i.e.* no measurement of temperature, pressure and CO_2 content of the air is required. In this paper, the principle of the two-wavelength absolute distance meter is explained, and preliminary results are presented, for each wavelength and with air refractive index compensation.

I. INTRODUCTION

The construction of large-scale facilities such as particle accelerators (Gervaise, 1983), the monitoring of civil engineering structures such as dams and tunnels (Curtis, 1992), or the survey of geological formations such as glaciers (Fruckacz *et al.*, 2016), volcanoes and faults (USGS, 2021) require absolute measurements of long distances with high accuracy. Therefore, we are developing an Absolute Distance Meter (ADM) that will bring metrologically traceable measurements for distances of several kilometers. The objective is to achieve an accuracy of 1 mm up to 5 km and beyond.

This instrument, an Electro-optical Distance Meter (EDM), is based on a well-known technique: a light beam is intensity modulated by a RF carrier, propagated in air up to a distant target, retroreflected, and finally detected by a photodetector. The distance to be measured is thus proportional to the phase delay φ measured between the RF carrier detected after propagation in air and the emitted one (Eq. 1):

$$D = \frac{1}{2}\left(\frac{\phi}{2\pi} + k\right) \times \frac{c}{n \times f_{RF}} \qquad (1)$$

with *c* the speed of light in vacuum, *n* the group refractive index of air, f_{RF} the frequency modulation of the light, and *k* an integer number corresponding to the number of times that the phase has rotated by 2π during its propagation.

The major challenge for such EDMs when used for the surveying of long-distances lies in the determination of the air refractive index. Usually, it is calculated using the semi-empirical Edlén's equation (Edlén, 1966, or similar updated formulas like Bönsch and Potulski, 1998) that depends on the vacuum optical wavelength, but also on the air temperature *T*, the pressure *p*, the partial pressure of water p_ω, and the CO_2 content *x*. The air refractive index is the parameter that contributes the most to the uncertainty on long-distance measurements: for instance, an accuracy of 1 mm over 5 km would require a knowledge of the temperature at 0.2 °C, which is nearly impossible to achieve in practice using classical sensors.

II. TWO-COLOUR ADM

A. *Principle*

To overcome this limitation, a two-colour system can be adopted (Earnshaw *et al.*, 1967). This consists in measuring two optical distances simultaneously at two different wavelengths. Thus, by using the dispersion relation between these two measurements, a compensation of the air refractive index can be applied (first velocity correction). This approach has led to a field instrument in the 1980's called Terrameter, which was able to measure a distance of 10 km with an uncertainty of 1 mm. It worked at wavelengths of 441.6 nm and 632.8 nm (Huggett, 1981; Gervaise, 1983). In the same period, a two-color Geodimeter was also developed: the performances were similar with an uncertainty of approximately 1.2 mm for a 10 km baseline (Langbein, 1987). However, these EDMs, produced in very limited series, are no more in operation because of their quite difficult use and of their complicated design.

The distance *L* measured by a two-colour ADM, *i.e.* the length of the wave paths also called air index

compensated distance (first velocity correction), is calculated as follows (Eq. 2):

$$L = D_{\lambda_1,n=1} - \frac{n(\lambda_1,T,p,x,p_\omega) - 1}{n(\lambda_2,\dots) - n(\lambda_1,\dots)}\left(D_{\lambda_2,n=1} - D_{\lambda_1,n=1}\right) \quad (2)$$

with $D_{\lambda_1,n=1}$ and $D_{\lambda_2,n=1}$ the two optical distances measured by the ADM at the wavelengths λ_1 and λ_2. The optical distances $D_{\lambda_1,n=1}$ and $D_{\lambda_2,n=1}$ are measured in open air, taking in Equation 1 an air index equal to 1. They are defined as (Eq. 3):

$$L = \frac{D_{\lambda_1,n=1}}{n(\lambda_1,T,p,x,p_\omega)} = \frac{D_{\lambda_2,n=1}}{n(\lambda_2,T,p,x,p_\omega)} \quad (3)$$

According to Meiners-Hagen (Meiners-Hagen and Abou-Zeid, 2008), and using the Bönsch and Potulski (1998) notations, the compensated distance can be simplified as follows (Eq. 4):

$$L = \frac{K(\lambda_1)D_{\lambda_2,n=1} - K(\lambda_2)D_{\lambda_1,n=1}}{K(\lambda_1) - K(\lambda_2) + p_\omega \times \left(g(\lambda_1) \cdot K(\lambda_2) - g(\lambda_2) \cdot K(\lambda_1)\right)} \quad (4)$$

where K and g are wavelength-dependent factors. It appears that the formula giving the compensated distance no longer depends on the temperature, pressure or CO_2 content, but only on the measurement of the partial pressure of water p_ω. To reach an accuracy of 1 mm over 5 km, p_ω has to be measured with an accuracy of 200 Pa, *i.e.* a relative humidity of 15.0 % at 10 °C or of 7.5 % at 20 °C.

In dry air, Equation 2 can be simplified as follows (Eq. 5):

$$L = D_{\lambda_1,n=1} - A(\lambda_1,\lambda_2) \times \left(D_{\lambda_2,n=1} - D_{\lambda_1,n=1}\right) \quad (5)$$

with (Eq. 6):

$$A(\lambda_1,\lambda_2) = \frac{K(\lambda_1)}{K(\lambda_1) - K(\lambda_2)} \quad (6)$$

Thus, for a given uncertainty on $D_{\lambda_i,n=1}$, the final uncertainty on the compensated distance L is degraded due to the factor A. Since this factor is considerably higher than unity, the uncertainty component due to the uncertainties on $D_{\lambda_1,n=1}$ and $D_{\lambda_2,n=1}$ is (Eq. 7):

$$\sigma(L) \simeq A \times \sqrt{\sigma\left(D_{\lambda_1,n=1}\right)^2 + \sigma\left(D_{\lambda_2,n=1}\right)^2} \quad (7)$$

when assuming the distance measurements performed at λ_1 and λ_2 are uncorrelated. It should be noted that even for wet air the scaling of the uncertainty by the factor A remains a good approximation.

B. *Design of the prototype*

This approach has been implemented at 779.8 nm and 1559.6 nm. The low dispersion between these wavelengths leads to a rather large factor A equal to 48. Thus, at each single-wavelength, an uncertainty around 20 µm on the distance measurement is required to reach an uncertainty of 1 mm on the air index compensated distance. Dealing with such a large factor A is for sure challenging. It could be reduced by choosing shorter wavelengths or by increasing the spacing between them. Thus, from a theoretical point of view, the two-colour Terrameter and Geodimeter EDMs, with blue and red lights, lead to potential better uncertainty thanks to a factor A around 22. Nevertheless, the wavelengths of our prototype are interesting due to the wide availability of affordable fiber-optic components in this range, especially at 1560 nm, which is used in the telecommunication industry.

The developed prototype is presented in Figure 1. It is compact, easily transportable, and thus ready for measurements in the field.
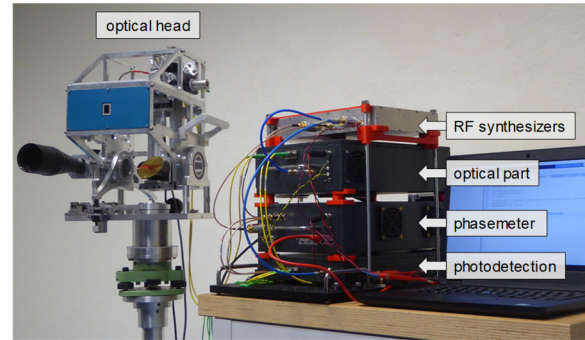

Figure 1. Photograph of the developed two-colour Absolute Distance Meter.

The setup of the two-colour telemeter is depicted in Figure 2. The optical carrier at 1560 nm is emitted by a laser diode, intensity-modulated by a RF carrier at 5060.75 MHz using an Electro-Absorption Modulator (EAM), then amplified by an optical amplifier. From this first signal, a second one at 780 nm is obtained by frequency doubling in a non-linear Periodically Poled Lithium Niobate (PPLN) waveguide. This second-harmonic generation results in a signal of half the wavelength of the pump at 1560 nm, but of modulation frequency unchanged.

Each of these optical signals passes through an optical splitter which acts as a high-isolation circulator. The two optical beams are then combined: after emission in free space and collimation by off-axis parabolic mirrors, the beam at 1560 nm passes through a dichroic mirror, while the one at 780 nm is reflected on it. Once the beams are superimposed, the spot sizes are magnified by a factor 10.2 thanks to a couple of parabolic mirrors to obtain, respectively, diameters of 28.0 mm and 29.0 mm (defined as twice the distance from the spot center where the intensity drops to $1/e^2$ of the max value) at 780 nm and 1560 nm.

After propagation over a long distance up to a hollow corner cube, the two beams come back to the telemeter to be reinjected into the same fibers as previously. After a second pass through the optical

splitters, the two laser beams are directed towards their respective photodiode (PD). At this point, the RF signals are down-converted by a Local Oscillator (LO) into an Intermediate Frequency (IF) of 10.75 MHz, amplified by 70 dB, and finally converted by 14 bit and 250 MSa/s Analog to Digital Converters (ADC). The distances are then calculated from the phase difference between these measurement signals and an electrical reference built from the direct mixing of the RF and LO carriers. The signals are processed digitally by a Field-Programmable Gate Array (FPGA) and displayed on Matlab.
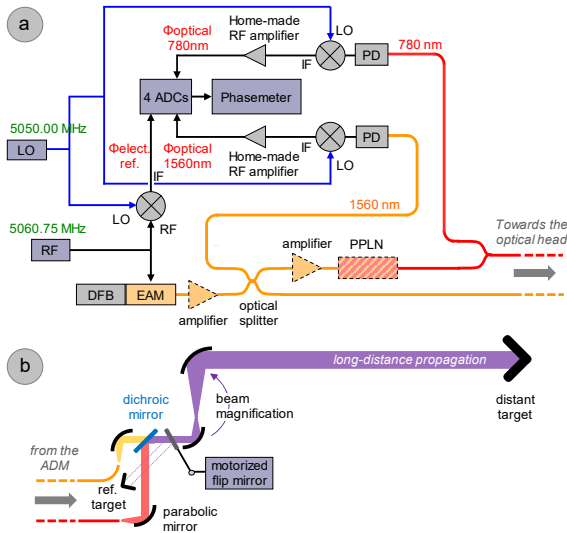
Figure 2. The two-colour fiber-optic Absolute Distance Meter (a), and its optical head for combination and collimation of the two optical beams, 780 nm and 1560 nm (b).

As shown in Figure 2, a motorized flip mirror has been implemented to deviate the free-space optical beams towards a small reference corner cube and thus compensate the phase variations induced by temperature changes in the optoelectronic, fibre-optic and microwave components. In practice, this mechanical zero measurement is performed every second.

It has to be noted that the distance resolution of our instrument is a function of the frequency modulation of the light: the higher the modulation frequency, the better the resolution. With a RF carrier around 5 GHz, a good compromise between cost and performances is obtained. For comparison, the two-colour Terrameter et Geodimeter EDMs had a RF carrier around 3 GHz (Gervaise, 1983; Langbein *et al.*, 1987).

At the end, the traceability of the measurement to the SI (Système International d'unités) is ensured by the knowledge of the modulation frequency and of the phase measurement. All the frequency synthesizers and the phasemeter are locked on a same reference, a Rubidium atomic clock accurate at 4.8×10^{-10} over a year (aging rate df_{RF}/f_{RF} of a Microsemi clock SA.22c).

As an example, a short distance of 0.5 m has been measured in a controlled environment (T = 23.6 °C).

Figure 3 shows the results for both wavelengths, 780 nm and 1560 nm, and for an air refractive index equal to 1. This depicts the distances calculated from Equation 1, in relative for a better reading of the curves. However, the absolute distances are known.
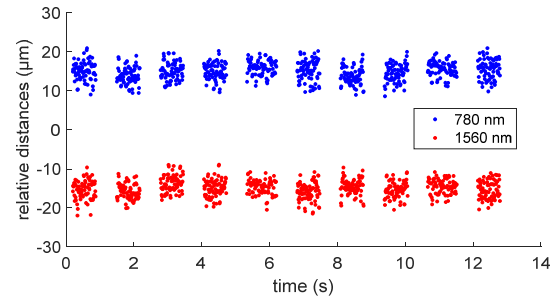

Figure 3. Distance measurement at 780 nm and 1560 nm over 0.5 m for n=1.

In Equation 1, the measured RF phase delay is wrapped into the interval $[-\pi, +\pi]$, therefore the integer number k of synthetic wavelengths c/f_{RF} has to be determined. In practice, the latter was deduced from several distance measurements performed at different RF carriers. In the example of the Figure 3, k equals to 17 and the measured distance to about 0.515 m.

For each measurement, 10 packets of 75 points (20 ms of integration time per point) have been recorded. Between these packets, a distance measurement of the reference target was performed to compensate for possible distance variations. At the end, the standard deviation of these curves is around 2.3 µm. However, the two distance measurements are in part correlated as the standard deviation of their difference is only 1.5 µm.

Figure 4 depicts the result after applying Equation 4, *i.e.* with air refractive index compensation. Due to the factor A, and as described by the Equation 7, the uncertainty is 48 times higher than the difference obtained between the two wavelengths: the observed standard deviation is equal to 69.6 µm. Nevertheless, in such a case, the knowledge of the air temperature and atmospheric pressure is not required to determine the compensated distance.

III. Experimental measurements

A. *1560 nm: comparison with an interferometric bench*

In the developed system, the optical carrier at 780 nm and its frequency modulation are generated from the modulated signal at 1560 nm. Therefore, as a prerequisite, it is necessary to ensure the correct functioning of the distance measurement at this wavelength. To this end, the ADM at 1560 nm has been compared to a 50 m-long interferometric bench, indoors, in a controlled environment. In this comparison, realized before the full completion of the prototype design, the optical beam at 1560 nm was directly collimated without passing through the dichroic mirror.
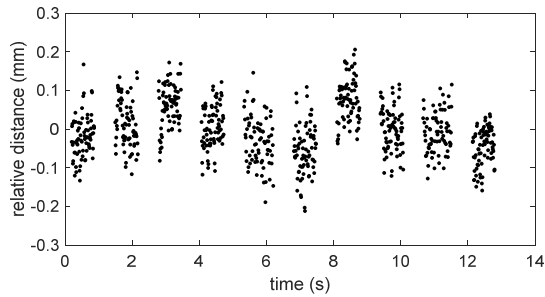
Figure 4. Distance measurement with air refractive index compensation over 0.5 m.

The results are depicted in Figure 5. The error (y-axis) represents the difference between the interferometric distance and an average distance over 10 packets measured by our ADM (like in Figure 3). Both distances have been corrected by the air refractive index, which has been estimated for the ADM wavelength (group index at 1560 nm) and the interferometric wavelength (phase index at 633 nm, Renishaw XL-80) thanks to weather stations. The displacement (x-axis) vary up to 100 m thanks to a double round trip.
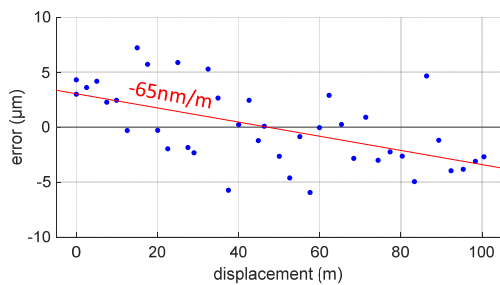
Figure 5. Comparison with an interferometric bench: errors for displacements up to 100 m.

Finally, we observe a standard deviation on the errors of 3.5 µm. However, after a linear regression, we obtain a slope of -65 nm/m. The uncertainties on the measured distances are mainly due to the uncertainties on the phase refractive index at 633 nm for the interferometer and the group refractive index at 1560 nm for the ADM, which are about $2 \cdot 10^{-8}$. The combined uncertainty is so around $3 \cdot 10^{-8}$, which could partly explain the observed slope. Further studies have shown that this slope is in fact dependent on time, not on the measured distance. Indeed, small temporal drifts can occur during the measurement time and induce the slope observed in Figure 5. This point is detailed in the next Section III B.

Once this slope is removed, the standard deviation on the errors is reduced to 2.9 µm. As shown in Figure 6, the error has also been measured for small displacements within the 3-cm synthetic wavelength of the system for distances around 0 m and 1.9 m. No cyclic error is present. This demonstrates an uncertainty around 3 µm for the two-colour system when it is used at 1560 nm.
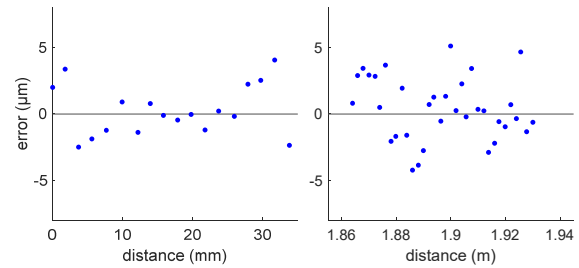

Figure 6. Comparison with an interferometric bench: small displacement steps to demonstrate absence of cyclic error.

At this moment, the second distance measurement at 780 nm has not been compared yet to an interferometric bench.

B. 2-colour: long-term stability over 1 m

As explained previously, with a factor A of 48, the uncertainty on the distance difference between the two wavelengths must be lower than 20 µm to reach an uncertainty better than 1 mm after the air refractive index compensation. Thus, as a first step, the stability of this distance difference has been evaluated over several days, for a fixed distance of 0.5 m and temperatures that vary between 5.5 °C and 23.6 °C. Results are depicted in Figure 7.
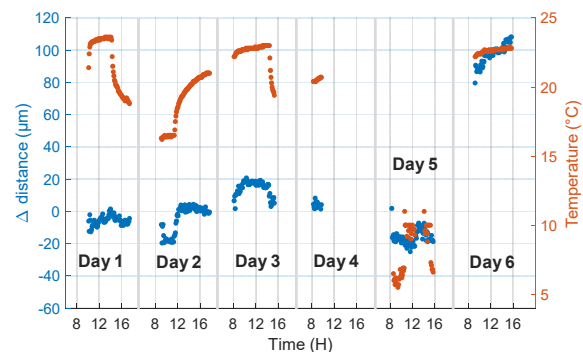

Figure 7. Evolution of the distance difference between the two wavelengths for a fixed distance, but different temperatures.

The variations of the distance difference between the two wavelengths are negligible at a fixed temperature, but when the temperature changes, variations of about 40 µm are observed over the first five days. On day 5, the instrument was installed outdoors with temperatures below 10 °C. When it returned inside the building on day 6, the thermal shock produces a huge change in the distance difference up to 130 µm.

It could appear obvious to attribute these variations to the thermal expansion of the components of the optical head made of aluminium (linear thermal expansion around 21 µm/m/°C), but the reference corner cube that compensates for the distance variations induced by temperature changes has been set up after the beam combination. Thus, by design, we should not observe drifts at this level of magnitude.

The origin of these drifts has been identified. Multiple reflections of the optical beam at 1560 nm inside the

dichroic mirror (designed with parallel faces) induce some crosstalks, *i.e.* the addition of a spurious signals to the ideal measurement signal, which change the measured phase delay φ in Equation 1. Thus, it is planned in the short term to change the dichroic mirror for a new one designed with a slight wedge form to eliminate the effects of these reflections.

These instabilities currently limit the uncertainty of our ADM to several millimeters (error of 6.2 mm for the 130 µm drift in Figure 7). However, as the distance difference between the two wavelengths remains quite stable in the absence of thermal shock, it is already possible to test the air refractive index compensation for the temperature variations that can occur outdoors.

C. *Instrument resolution over 5.2 km*

The developed instrument was tested over 5.2 km, above a dense urban area. The two-colour ADM was located in Paris, on the rooftop of the Laboratoire National de métrologie et d'Essais (LNE) building, at 22 m above the ground, while the target was located in Meudon, in a public park at ground level. The target was a hollow corner cube with enhanced aluminum coating and 127 mm clear aperture.

As a first step, the resolution of the developed system has been estimated. To this end, the distant target has been mounted on a translation stage, then it has been displaced by a small step of 3.5 mm once every 30 seconds. This measurement took place on 7th April 2021, a day with an overcast sky, a wind of about 14 km/h. In Paris, the temperature was around 12.0 °C, the relative humidity was equal to 33 %, and the atmospheric pressure to 1025.2 hPa. The results are depicted in Figure 8 at each wavelength.
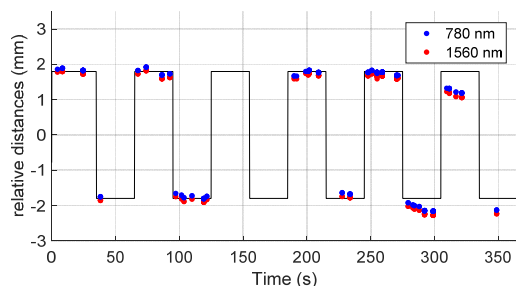

Figure 8. The measured distance displacements at each wavelength, 780 nm and 1560 nm, with no air refractive index compensation.

For a proper operation of the phasemeter, we have selected data with RF amplitudes between -25 dBm and +0 dBm for the wavelength at 780 nm, and between -15 dBm and +0 dBm for the wavelength at 1560 nm. Since there is no correction of the air refractive index in Figure 8, a distance drift up to 0.6 mm can be observed for each wavelength, especially after 275 seconds. However, the distance difference between the two measured distances is stable over this period with a standard deviation of only 13.4 µm (or 11.3 µm if the

points measured after 275 s are ignored). As shown in Figure 9, the distribution of this difference presents a gaussian shape.
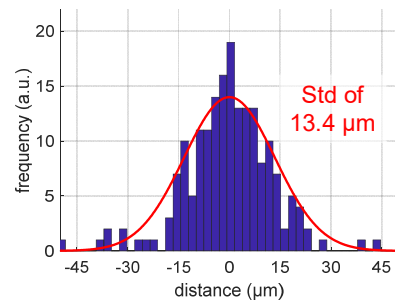

Figure 9. Distribution of the distance difference between the two wavelengths.

Lastly, Figure 10 depicts the results after air refractive index compensation, *i.e.* after the application of the Equation 4. This demonstrates that the two-colour system is able to distinguish the movements of a distant corner cube with has a resolution around 500 µm, without the need to know the air temperature and the pressure, but only the partial pressure of water.
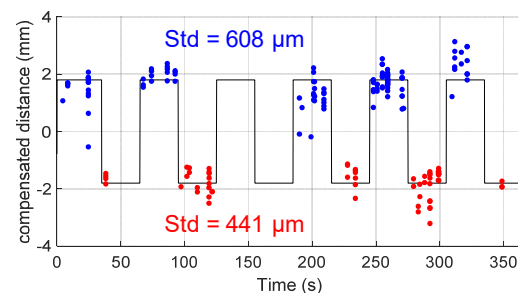

Figure 10. The measured distance displacements with air refractive index compensation.

The distribution of the results of Figure 10 has also been plotted as a histogram and fitted with two gaussian curves in Figure 11. The distance between the peaks of each gaussian curve is, as expected, equal to 3.5 mm.
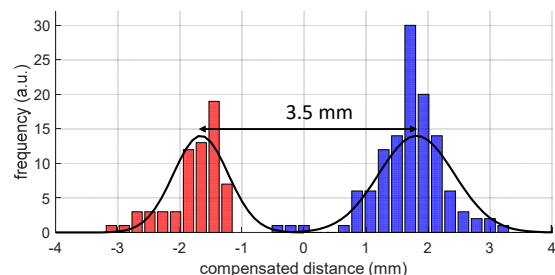

Figure 11. Distribution of the compensated distance measurements for a displacement of the target of 3 mm.

D. *Air index compensation over 5.2 km*

As a second step, the ability of the two-colour ADM to compensate for temperature and pressure variations over 5.2 km has been estimated. The measurement took place on 8th December 2021, a day with a sky

partially overcast, a moderate wind of about 15 km/h, and a rising atmospheric pressure between 989 hPa and 991 hPa. As shown in Figure 12, the temperatures measured at Paris and at Meudon are in relative agreement with a maximum difference of 2°C between the two sites. However, the relative humidities can differ up to 18%.
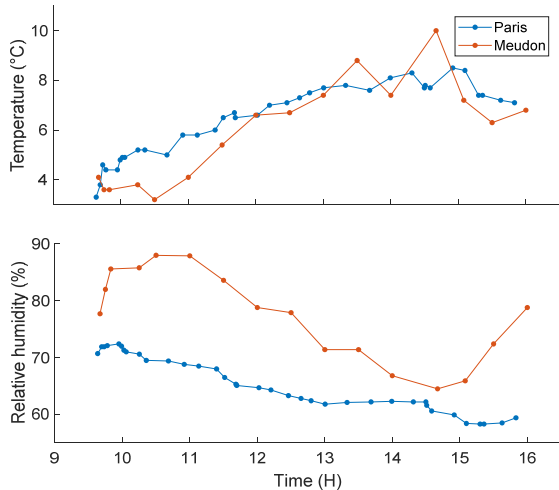

Figure 12. Evolution of the temperatures and relative humidities.

The value of the distance was unknown, so only the ability of the instrument to compensate from variations of the atmospheric parameters has been verified, not its accuracy. To this end, 30 continuous distance records were made between 9 a.m. and 4 p.m., each lasting between 1 min and 10 min. The signals detected after a 2×5.2 km round trip was not subject to large variations thanks to a day of low sunlight, and therefore of limited scintillations. For a proper operation of the phasemeter, we have selected data with RF amplitudes between -18 dBm and +0 dBm for both wavelengths. This represents 5% of the captured distances.

The results are presented in Figure 13 for each wavelength taken separately and for an air refractive index equal to 1. A drift of -14.5 mm can be observed during the day, which could be explained by an increase of the temperature of 2.9°C or a fall of the pressure of 10.3 hPa. In practice, it can be assumed that the variations of the measured pressures were relatively correct, which means that the real variations of the air temperature integrated over 5.2 km were probably less than the ones measured at each end of the baseline.

The shorter is the wavelength, the larger is the index n, and the greater will be the distance measured for n=1. Thus, the optical distance at 780 nm is about 3 cm longer than the one at 1560 nm. Moreover, as depicted in Figure 14, this difference between the two wavelengths evolves during the day, up to 300 μm, due to changes in temperature and pressure.

In order to deduce the compensated distance, the Equation 4 has been applied. To this end, the partial pressure of water, p_ω, was calculated from the values provided by the weather station located in Paris, more

stable during the day than the ones located at the opposite side of the baseline. The result of the application of Equation 4, *i.e.* the air index compensated distance, is depicted in Figure 15.
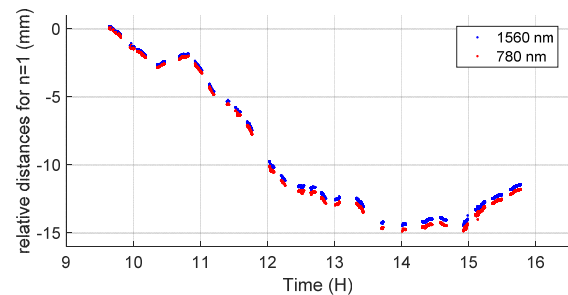

Figure 13. Distance measurement at 780 nm and 1560 nm for n=1 over 5.2 km.
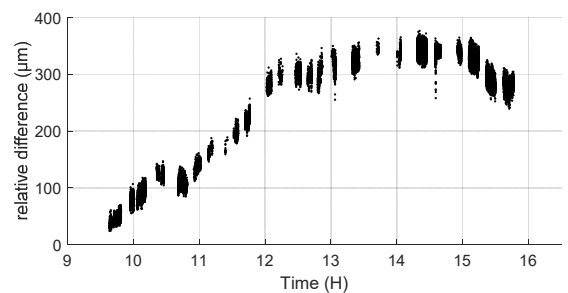

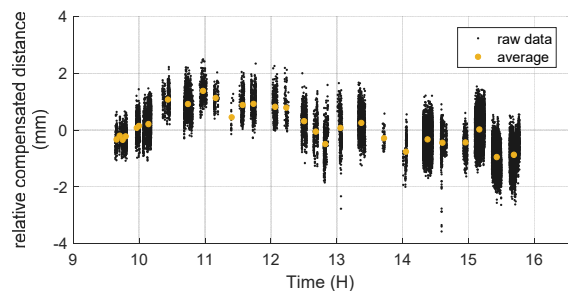Figure 14. Distance difference between the two wavelengths.

Figure 15. Distance measurement with air refractive index compensation.

To reach an uncertainty of 500 μm over 5 km, p_ω has to be measured with an uncertainty of 100 Pa, *i.e.* an uncertainty on the relative humidity of 7.5 % at 10 °C. Measuring the humidity at a single point is therefore critical since we have observed for similar temperatures up to 18 % difference between Paris and Meudon.

For a given distance record, the standard deviation on the raw data is typically around 420 μm. However, the average value of these records varies of 2.3 mm peak-to-peak (yellow points in Figure 15). These variations probably come from a drift of 40 μm between the two wavelengths as highlighted in Figure 7, or a bad estimate of the variations of the relative humidity of air.

Lastly, it has to be underlined that the stability of the building from where the distance measurements were performed in Paris has been measured. This was done using a digital level located at the ground level, a Leica DNA03, aiming at vertically, 22 m above thanks to a

deflector prism at its output, an invar levelling staff mounted on the roof of the building, horizontally in the direction of the baseline. According to the monitoring method, the possible instability of the building in the baseline direction was found to be less than 0.3 mm.

IV. Conclusion

We have developed a prototype of two-colour ADM. The latter, still under development, already shows promising preliminary results.

Indoors, in a controlled environment and for the wavelength at 1560 nm, an accuracy of 3.5 µm has been demonstrated for distances up to 100 m. The second wavelength has yet to be characterized, but if similar results are obtained, this will lead to an uncertainty around 240 µm after air refractive index compensation.

Outdoors, over 5.2 km, the resolution of the instrument is around 500 µm with air refractive index compensation. This compensation was tested over 6 hours, with temperature and pressure variations of 7 °C and 2 hPa, respectively. This has demonstrated that a distance of 5.2 km can be measured without the knowledge of either the temperature or the atmospheric pressure: the peak-to-peak variation was only 2.3 mm. However, it is important to notice that these measurements were carried out under favourable weather conditions, *i.e.* days with low sunlight and so low atmospheric perturbations.

The crucial point to improve is the stability of the measured distances to reduce the residual drift between the two wavelengths. This limits the reproducibility of the current design to about 6 mm when large temperature variations occur. Nevertheless, the origin of this instability has been identified and should be greatly reduced by a new optical design. Once this is achieved, the accuracy will be estimated by a comparison with an interferometric bench for short distances up to 100 m and with the Nummela reference baseline for long distances up to 864 m (Jokela and Häkli, 2006). Lastly, a comparison with global navigation satellite systems (GNSS) will be carried out for longer distances, up to several kilometers.

V. Acknowledgements

References

Bönsch, G., and E. Potulski (1998). Measurement of the refractive index of air and comparison with modified Edlén's formulae. In: *IOP Metrologia*, Vol. 35, No. 2, pp. 133-139.

Curtis, C. J. (1992). Calibration and use of the Mekometer ME5000 in the survey of the Channel Tunnel. In: *Proc. of the Workshop 'the use and calibration of the Kern ME5000 Mekometer'*. Stanford Linear Accelerator Center, Stanford University, Stanford, California, USA, pp. 67-82.

Earnshaw, K. B., and J. C. Owens (1967). Dual wavelength optical distance measuring instrument which corrects for air density. In: *IEEE Journal of Quantum Electronics*, Vol. 3, No. 11, pp. 544–550.

Edlén, B. (1966). The Refractive Index of Air. In: IOP Metrologia. Vol. 2, No. 2, pp. 71-80.

Frukacz, M., R. Presl, A. Wieser, and D. Favot (2016). Pushing the Sensitivity Limits of TPS-based Continuous Deformation Monitoring of an Alpine Valley. In: *Proc. Of the 3rd Joint International Symposium on Deformation Monitoring (JISDM)*. Vienna, Austria.

Gervaise, J. (1983). First results of the geodetic measurements carried out with the Terrameter, two wavelength electronic distance measurement instrument. In: *Proc. of 'Geodätischen Seminar über Electrooptische Präzisionsstreckenmessung'*. Munich, Germany, pp. 213-229.

Huggett, G. R. (1981). Two-Color Terrameter. In: *Developments in Geotectonics*, Vol. 16, pp. 29-39.

Jokela, J., and P. Häkli (2006). Current Research and Development at the Nummela Standard Baseline. In: *Shaping the Change, XXIII FIG Congress*, Munich, Germany.

Langbein, J. O., M. F. Linker, A. F. McGarr, and L. E. Slater (1987). Precision of two-color geodimeter measurements: Results from 15 months of observations. In: *Journal of Geophysical Research*, Vol. 92, No. B11, pp. 11644-11656.

Meiners-Hagen, K., and A. Abou-Zeid (2008). Refractive index determination in length measurement by two-colour interferometry. In: *Measurement Science and Technology*, Vol. 19, No. 8, 084004.

USGS (2021). Eathquake Hazards Program, consulted in 2021. Two-color Electronic Distance Meter (EDM). In: https://earthquake.usgs.gov/monitoring/deformation/edm/